

The Role of Microstructure on Ductility of Die-Cast AM50 and AM60 Magnesium Alloys

GURJEEV CHADHA, JOHN E. ALLISON, and J. WAYNE JONES

Die-cast AM50 and AM60 magnesium alloys have been examined to determine the fracture processes in bending and tension and to elucidate the influences of microstructure and porosity distribution on mechanical properties. The effect of section thickness has been explored using 2-, 6-, and 10-mm-thick die-cast plates. The processes of damage accumulation in terms of crack initiation, growth, and linkage leading to eventual failure have been studied qualitatively using progressive tensile straining experiments and three-point bend studies. The presence of a heterogeneous distribution of porosity played a critical role in the observed differences between strains to fracture in tension and in bending. More rapid damage accumulation at lower strains was observed in the high porosity regions with the rate of damage accumulation strongly dependent on the loading mode. Fracture processes at the microstructural level were characterized by scanning electron microscopy using an in-situ bending fixture. Crack initiation and growth occurred predominantly in the interdendritic eutectic regions, both in the presence of porosity and, to a lesser extent, in pore-free regions. The role of porosity volume fraction and distribution on ductility in these alloys has been examined using a modified Brown-Embury model. This model allows the prediction of fracture location in either loading mode by predicting the critical strains for the onset of cracking in differently strained regions of the test samples.

DOI: 10.1007/s11661-006-9027-z

© The Minerals, Metals & Materials Society and ASM International 2007

I. INTRODUCTION

DIE-CAST magnesium alloys have been receiving considerable attention from the automobile industry because of their combination of good mechanical properties, low density ($\sim 1.8 \text{ g/cm}^3$), and high-speed production of complex parts.^[1-4] For applications demanding good ductility, the AM (Mg-Al-Mn base) series alloys are used, whereas, for strength-sensitive applications, the AZ91D (Mg-Al-Zn base) and other alloys are preferred.^[2,5-7]

The present study investigates two of the prominent high-pressure die-cast alloys, AM50 and AM60, that are used in applications requiring good ductility. High-pressure die casting is characterized by rapid die filling, cooling, and solidification of the metal in the die with considerable microstructural variability associated with selection of process parameters. The microstructure of high-pressure die-cast AM alloys consists of α -Mg dendrite cells, externally solidified α -Mg dendrites, and a divorced-eutectic (α -Mg + β -Mg₁₇Al₁₂).^[2,6-9] A few spherical Mn-rich intermetallic particles are also generally observed in the microstructure. Close to the die walls, a porosity-free region is often reported. This

region consists of very fine α -Mg dendrites with a cell size approximately 5 to 7 μm and is termed the "skin" or near-surface region. This region has a fine dendrite cell size and an absence of porosity. It, therefore, has higher strength and ductility than the interior regions of the castings.^[10] The near-surface region thus imparts good mechanical properties required for structural applications, especially in thin casting sections.

Large, externally solidified α -Mg dendrites formed due to premature solidification in the sleeve region are observed at the center of all the castings. They are distinguishable from the primary α -Mg dendrites because of their much larger cell size and have equivalent circle diameter of 10 to 12 μm .^[8] The presence of these externally solidified dendrites in the casting results in a bimodal α -Mg grain size distribution for these alloys.^[5,6,8]

The die filling process leads to formation of bands where porosity is distributed heterogeneously with deleterious effects on strength and ductility.^[11] Models have been proposed explaining the formation of these porosity segregation zones (PSZs). A model based on relative strength distribution across the casting and the presence of externally solidified crystals at the center flowing relative to the solidification front from the die wall has been proposed.^[12-14] Recently, another model was proposed that argues that the presence of externally solidified crystals at the center and a pressure drop in the liquid are necessary for PSZ formation.^[15]

The mechanical properties of these alloys are well characterized with most studies correlating mechanical properties with bulk porosity.^[6,16-18] As AM60 has a higher volume fraction of the β -Mg₁₇Al₁₂ phase than

GURJEEV CHADHA, Senior Design Engineer, is with the Device Physics and Modeling Group, Spansion LLC, Sunnyvale, CA 94088, USA. Contact e-mail: gurjeev.chadha@spansion.com. J. WAYNE JONES, Arthur F. Thurnau Professor, is with the Department of Materials Science and Engineering, University of Michigan, Ann Arbor, MI 48109, USA. JOHN E. ALLISON, Senior Technical Leader, is with the Research and Advanced Engineering, Ford Motor Company, Dearborn, MI 48124, USA.

Manuscript submitted May 11, 2005.

AM50, because of its slightly higher aluminum content, it generally exhibits slightly lower ductility than AM50.^[2,7] There is general agreement that ultimate tensile strength and tensile ductility decrease with increasing bulk volumetric porosity, as measured using the Archimedes method.^[16–18] However, some authors^[6,17,18] report no effect on 0.2 pct yield strength with increasing porosity, while others have reported a linear decrease.^[16] The issue of a critical level of bulk porosity has also been addressed in the literature^[18] and it has been reported that, for very low (<0.5 to 1.5 vol pct) bulk volumetric porosity levels, there is little variation in yield strength and ultimate tensile strength with ductility.^[6,18]

An understanding of the effect of section thickness on mechanical properties is also lacking.^[6,8,19–22] The section thickness itself does not directly affect the mechanical properties, but it influences the solidification conditions that lead to the variations in the as-cast microstructures that translate to variation in mechanical properties. Rodrigo *et al.*^[6] and Bowles^[8] have reported that ductility increases with increasing section thickness. On the other hand, Stich and Haldenwanger^[21] and Schindelbacher and Rösch^[22] reported a linear decrease in 0.2 pct yield strength, tensile ductility, and ultimate tensile strength. Easton *et al.*^[19] and Abbott *et al.*^[20] observed an increase in ductility when section thickness increased from 1 to 5 mm and decreased between 5 and 10 mm. Although there is general agreement on the influence of section thickness variation on mechanical properties in all of these studies, an understanding of the microstructure-property correlation is still lacking. Furthermore, studies of mechanical behavior in bending have not been performed for these alloys,^[23] and there is a lack of quantitative data for both AM50 and AM60 in the literature for this important loading mode.

While a heterogeneous distribution of porosity has a deleterious effect on mechanical properties at the macroscale, the brittle eutectic phase is critical to deformation at the microstructure level.^[24] This understanding is important because the eutectic α -Mg and β -Mg₁₇Al₁₂ microconstituents are believed to be critical in the fracture of these alloys.^[8,24,25] Bowles^[8] most recently showed that the fracture process becomes increasingly intergranular with the crack paths following the eutectic region in aged AZ91D compared to the combination of intergranular and transgranular modes in the as-cast condition. A complete understanding of damage evolution in the interdendritic eutectic region is, therefore, necessary to better understand how to improve ductility in these alloys. This is especially important if process parameters can be controlled to eliminate porosity segregation, leaving eutectic morphology and dendrite arm spacing as the primary microstructural variables influencing ductility in these alloys.^[26] The eutectic microstructure of hypoeutectic magnesium-aluminum alloys exhibits a wide range of morphologies that depend on the aluminum content and the cooling rate.^[12,27] The morphology varies from fibrous or lamellar near the eutectic composition (33 wt pct Al) to granular, partially divorced and eventually to fully

divorced eutectic in alloys with less than 10 wt pct Al, which corresponds to the alloys in the present study.

In this study, we examine the phenomenon of damage accumulation during deformation, with special attention to the presence of a heterogeneous distribution of porosity and the role of the interdendritic eutectic microconstituent on the failure processes in both tension and bending. The influence of section thicknesses of 2, 6, and 10-mm on tensile properties and fracture behavior for both AM50 and AM60 are examined. These thicknesses are representative of the section thickness variation in die-cast automotive components. Finally, a modified Brown–Embury model is presented that accurately predicts the ductility of these alloy plates in tension and that has been extended to predict both failure location and ductility in bending.^[28,29]

II. EXPERIMENTAL PROCEDURE

A. Material and Preparation

Die-cast plates with section thicknesses of 2, 6, and 10 mm were examined for both AM50 and AM60 (Figure 1). All die-cast plates were 126-mm long and 26-mm wide. The plates were obtained from Spartan Light Metals and were cast using a 700-ton cold chamber high-pressure die casting unit. The melt temperature was 677 °C and the die temperature was 95 °C. Compositional analysis was done for each plate thickness using the inductively coupled plasma technique, and the results are shown in Table I. The microstructure of different regions of die-cast plates was investigated by optical and scanning electron microscopy. Because of the relatively low hardness of magnesium, metallographic specimens were prepared by low-stress polishing on napless cloths. The final polishing step used a 0.05- μ m alumina powder suspension in Isocut fluid on a Chemomet pad, followed by etching in acetic glycol or 2 pct Nital solution.

Bulk porosity measurements were performed on regions of interest for all plates using the Archimedes

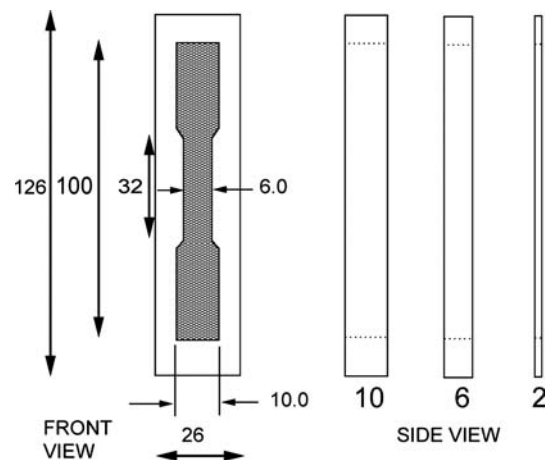


Fig. 1—Tensile test specimen geometry used for all of the section thicknesses.

Table I. Composition (in Weight Percent) for All Three Die-Cast Plates for AM50 and AM60

Elemental Composition (in Wt Pct)	AM50			AM60		
	2 mm	6 mm	10 mm	2 mm	6 mm	10 mm
Al	5.16	5.04	4.95	6.07	6.07	6.12
Mn	0.36	0.35	0.35	0.34	0.33	0.33

method.^[5,16,17] A random selection of machined specimens was sacrificed to measure volumetric porosity in the unstrained condition. For tensile specimens, porosity was measured in the gage region, and for bend test specimens, porosity was measured in the region just below the center pin. The liquid medium used in this study was chemical grade 2-propanol solution and measurements were done under stable ambient temperature conditions. Variation in the density of 2-propanol with ambient temperature was taken into consideration. Quantitative porosity measurements were also performed using the commercially available image processing tool kit (IPTK 4.0) on failed sections from the plates where bulk porosity could not be measured by the Archimedes method.

B. Mechanical Testing

Tensile tests and progressive strain tests were performed to understand the mechanical response and phenomenology of damage evolution in these alloys. Specimens were machined from rectangular cast plates of AM50 and AM60 for the three section thicknesses, as

shown in Figure 1. The die-cast surfaces were thus removed from the two side surfaces of each specimen but were left intact on the two specimen faces. A minimum of eight tensile tests was conducted at room temperature for each thickness at a strain rate of $5 \times 10^{-4} \text{ s}^{-1}$ using an Instron 5582 test machine. Tensile strains were measured using extensometers of 25.4- or 12.7-mm gage length.

Three-point bend tests were performed on the 6- and 10-mm-thick plates in the as-cast condition with the near-surface region intact on all edges and faces. The three-point bend configuration was chosen to better accommodate the dimensions of the die-cast coupons. Strains on the tensile surface are maximum at a position in line with the upper support beam and decrease away from this position. Thus, nominal strains are measured and reported here. Tests were performed using an Instron 5582 equipped with a simple bend test fixture, as shown in Figure 2. Failure was defined as a 5 pct drop in the load levels in the three-point bend test for both 6- and 10-mm section thicknesses. Loading to the 5 pct load drop was sufficient to produce surface cracks on the tensile faces of the plates. The 2-mm plate did not fail in this manner because geometrical limitations posed by the test fixture required tests to be terminated well before failure. Strains to failure were estimated by measuring the change in length of five equispaced lines 4 to 5 mm in length that were placed on the tensile side of the bend specimens prior to testing.

C. Progressive Straining

Surface observations of damage accumulation were made at increasing strain levels on the faces perpendicular to the thickness direction. The 6-mm-thick plates were selected for this study because they showed higher ductility, with relatively low scatter in ductility. Plastic strain levels of 1, 3, and 5 pct were chosen for detailed examination of the damage accumulation processes in the PSZs and in the near-surface regions at increasing levels of strain. Individual samples were strained to each of the target strain levels, load was removed, and the samples were then sectioned for microstructural examination. The cross sections illustrated in Figure 3 were metallographically prepared and examined in a PHILIPS XL30FEG using the backscatter detection mode.

D. In-Situ Bend Testing

Damage accumulation at the microstructural level was observed in a scanning electron microscope equipped with a three-point bend fixture. Rectangular specimens 63.5-mm long, 4-mm wide, and 3 mm in thickness were machined from the 6-mm AM50 and AM60 plates. The bend specimens were machined such that the tensile surfaces observed in the scanning electron microscope (SEM) were from the PSZ for some specimens and from the pore-free near-surface region for others. Specimens were metallographically polished and etched before straining in the SEM.

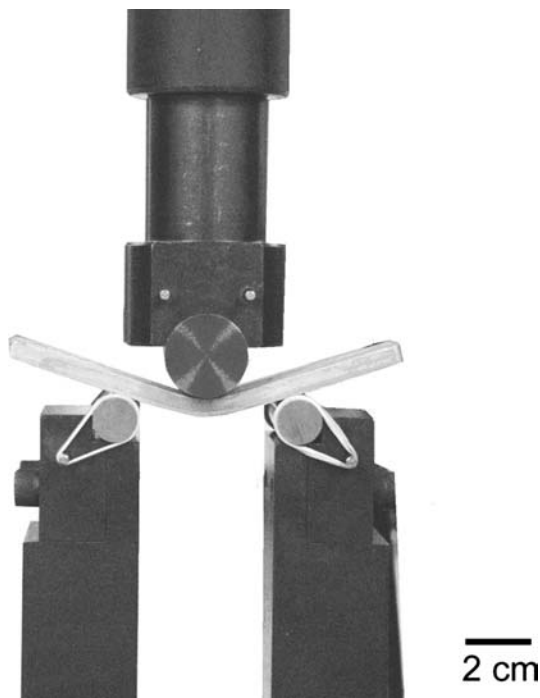


Fig. 2—Three-point bend test setup.

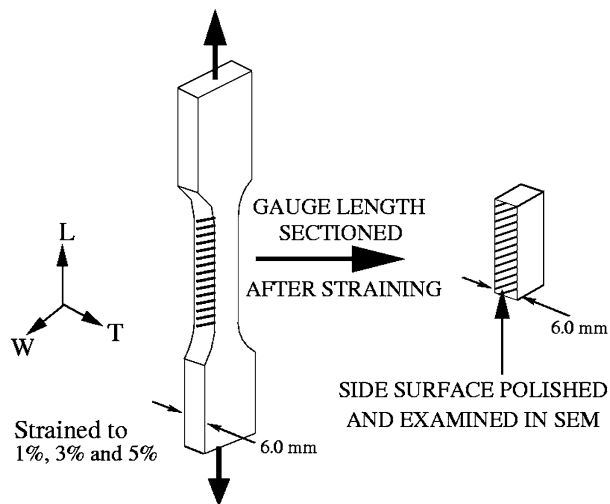


Fig. 3—Schematic showing sample preparation for observing progressively strained samples at 1, 3, and 5 pct. Plane of observation denotes the face metallographically polished and examined.

III. RESULTS AND OBSERVATIONS

A. Microstructure

As illustrated in Figure 4, the microstructure for all plates consists of primary α -Mg dendrite cells, externally solidified α -Mg dendrites, and a divorced-eutectic (α -Mg + β -Mg₁₇Al₁₂) in the interdendritic regions. The primary α -Mg dendrites form the largest portion of the microstructure and are surrounded by the divorced eutectic in a noncontinuous manner. A few round particles were also observed in the microstructure and were determined to be Mn-rich intermetallics by energy-dispersive X-ray analysis. Qualitative examination on a number of sections in all plate thicknesses showed the presence (Figure 4) of a bimodal dendrite/cell size distribution that is attributed to the presence of material that solidified before entering the die chamber.

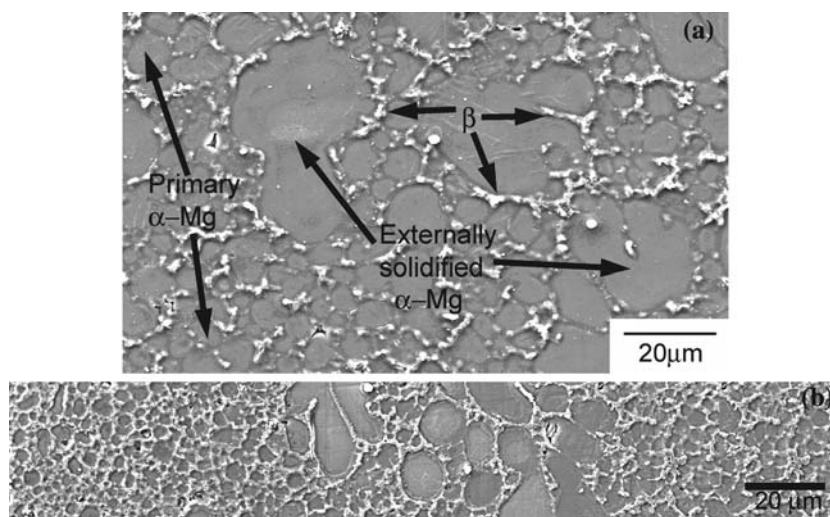


Fig. 4—(a) Photomicrograph showing the primary microstructural phases in these alloys. (b) Bimodal grain size distribution; note the difference in size of various α -Mg dendrites.

As shown in Figure 5, the low porosity near-surface region close to the die walls had a very fine grain size (less than $\sim 5 \mu\text{m}$) and the casting interior a larger grain size (~ 10 to $15 \mu\text{m}$). Porosity segregation zones were also observed in the interior of the castings for all the plates, as shown in Figures 5(a) and (b). The micrographs shown in Figure 5 are representative of all 2- and 6-mm plate thicknesses for both AM50 and AM60. For both alloys, the 10-mm-thick plates lacked a PSZ but had a high general pore volume fraction in the sample interior. The word “porosity” is used here without differentiating between shrinkage, microshrinkage, and gas-related porosity. However, the pores observed in all castings were primarily shrinkage, or a combination of gas and shrinkage, porosity that was concentrated at or near the casting centers and that consisted of either large pores or small, interdendritic micropores.

The porosity volume fraction was measured for each plate thickness using the Archimedes method and the results are given in Table II. The porosity volume fractions in gage sections of unstrained samples were also measured by the same method. As expected, the volume fraction of porosity increased with increasing section thickness. Essentially, all porosity was concentrated in the center region of the castings either in the form of individual shrinkage pores or in the PSZs. Little or no porosity was observed in the near-surface region.

The center regions of all three thicknesses for the AM50 plates are shown in Figure 6. The nominal pore size increases significantly as the section thickness increases, which correlates with the increasing volume fraction of porosity and longer solidification times. The 2- and 6-mm AM60 plates had no large pores, compared to those that were observed in AM50 plates that had a high porosity center region (compare Figures 6(b) and (d)). The bulk volumetric porosities of AM50 and AM60 were equivalent (Table II), which suggests that the porosity in AM60 has a more uniform distribution of small pores compared to AM50. Porosity measurements using the Archimedes

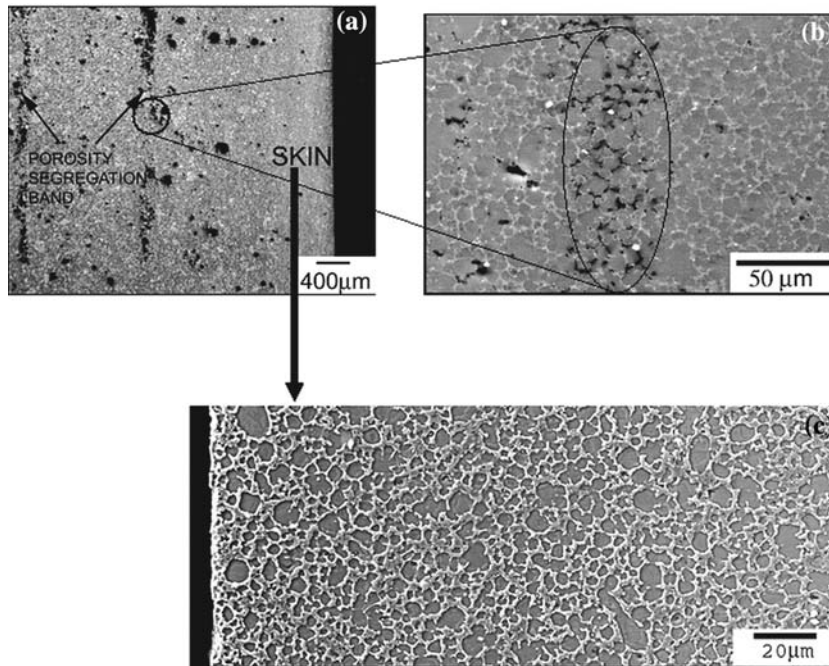


Fig. 5—(a) Porosity segregation band as seen in the AM50-6 mm plate; note the pore free skin region. (b) Closer look at the microporosity segregation zone in the backscattered electron mode. (c) Closer look at the fine dendrite size pore free skin region.

method were also made on the entire cross section for the 6- and 10-mm plates to correlate failure strains in bending with the volume percentage of porosity. For this, a few plates were sacrificed and sections were taken at midspan of the plates, corresponding to the region below the center pin in bend tests. Similar bulk volume fractions of porosity of 1 pct for the 6-mm plate and 2.5 pct for the 10-mm plate were recorded for both AM50 and AM60.

B. Mechanical Properties

Similar variations in mechanical properties with increasing section thickness were observed for AM50 and AM60. Strength and ductility decrease linearly as the section thickness increases for either alloy. The variation of ductility with increasing plate thickness is shown in Figure 7. The tensile properties for both AM50 and AM60 are listed in Table III. The mechanical properties determined in the present study (for both AM50 and AM60) are slightly lower than the values reported for these alloys in the literature.^[2,5-8] This difference may be attributed to the absence of the

fine-grained near-surface regions on two sides of the machined tensile specimen, as detailed in Section A.

Figure 7 shows that the ductility in bending for 6- and 10-mm plates is modestly higher for the AM50 plates. In tension, ductility is essentially the same for the 6- and 10-mm thicknesses and at 2-mm AM60 shows a slightly higher ductility. It is expected that AM50 would have the higher ductility^[2,7] because of its lower aluminum content and, hence, lower β -phase volume fraction. This behavior is attributed to the more highly localized regions of porosity in the AM50 castings (Figures 5 and 6(a) through (c)) compared to the more uniformly distributed porosity in the AM60 plates (Figure 6(d)). The variation of strain to fracture with bulk porosity is shown in Figure 8. For both AM50 and AM60 die-cast plates, strain to fracture decreases with increasing volume fraction of porosity.

Higher ductility is observed in bending tests than in tensile tests in 6- and 10-mm-thick plates for both AM50 and AM60 alloys, as shown in Figures 7 and 8. The bend ductility values reported are outer fiber failure strains and were approximately 15 to 17 pct for the 6-mm-thick plates, compared to tensile failure strains of approximately 7 to 9 pct. For the 10-mm-thick plates, ductility was much greater in bending (~12 to 14 pct) than in tension (~2 to 3 pct). Bend data for the 2-mm plates are not included, as the plates did not fail in the bend fixture. The high ductility in bending is expected, because, unlike in tension, the region under the highest strain is the near-surface region, which has negligible porosity and a very fine grain size. It should also be noted that the marker technique used to measure strain levels in bend plates gave an approximate lower bound of the actual

Table II. Average Bulk Porosity Levels in the Gauge Section for All Three Die-Cast Plates for AM50 and AM60

Plate Thickness (mm)	Porosity (Vol. Pct)	
	AM50	AM60
2	0.9 ± 0.1	1.0 ± 0.2
6	1.3 ± 0.2	1.5 ± 0.3
10	3.3 ± 0.2	3.6 ± 0.2

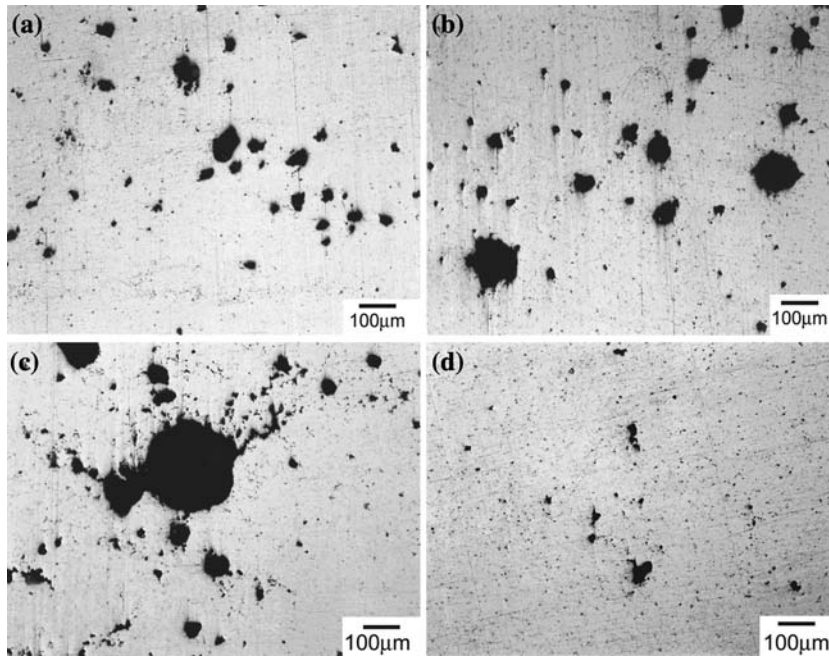


Fig. 6—Center region of the $(T) \times (W)$ cross section in AM50 alloys plates: (a) 2 mm, (b) 6 mm, (c) 10 mm, and (d) AM60-6-mm plate for comparison.

plastic strains at failure for both 6- and 10-mm-thick plates. Furthermore, as the stress on the tension side of the bend bar is not constant, as it would be in four-point bending, the measured bending strains should be considered as relative, not absolute, values.

C. Phenomenology of Deformation at the Macrostructure Level

Macroscale response to increasing strain levels of the PSZ and the near-surface region (Figure 9) was clearly elucidated by progressive strain tests (Figure 3). It was observed that damage accumulation occurred all along the gage length of the specimens and was localized primarily in the PSZ. Microcrack initiation appears to be aided by the sharp ends of the micropores, which act as significant stress/strain concentrators. The presence of other similarly nucleated microcracks from nearby

pores results in easy microcrack linkage, and long, sharp cracks form at strain levels as low as 1 pct. The size of the subcritical cracks increases with increasing strain levels and, for the 5 pct strained specimen, cracks as long as 1 mm are observed throughout the gage length. Damage accumulation, qualitatively defined by the number and size of cracks observed, was higher in AM50 than in AM60 at each strain level, especially for the 1 and 3 pct strained samples. For the 5 pct strained sample, similar levels of damage were recorded in both AM50 and AM60 and damage was, again, localized in the PSZ.

Damage accumulation in samples that failed in bending was characterized by appropriate sectioning of failed plates to reveal cracks and their propagation paths through the thickness for both 6- and 10-mm plates. For 6-mm-thick plates in both AM50 and AM60, failure initiated in the near-surface region and cracks propagated toward the specimen center. Multiple cracks also formed in the low-strength PSZ (Figures 10(a) and (b), shown by arrows) but did not cause failure. A different damage accumulation process led to failure in the 10-mm plates of AM50 and AM60. For these specimens, the higher pore volume fraction in the specimen interior favored the nucleation and coalescence of microcracks that subsequently propagated toward the specimen surface, causing failure, as shown in Figure 10(c). Damage accumulation at the macroscale arises from microscale events such as the formation and linkage of microcracks in the pore-rich zones. Crack extension from pores must necessarily involve microstructure-related fracture processes and is expected to be similar, if not identical, to fracture processes in pore-free regions of the microstructure. Therefore, fracture

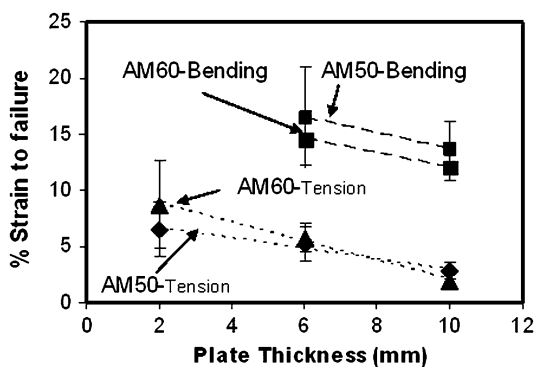


Fig. 7—Variation of tensile ductility and bend failure strains with plate thickness for both AM50 and AM60.

Table III. 0.2 Pct YS, UTS, and Pct Elongation for Various Section Thicknesses for Both AM50 and AM60 (Numbers in Parentheses Correspond to One Standard Deviation)

Plate Thickness (mm)	AM50			AM60		
	0.2 Pct YS (MPa)	UTS (MPa)	Pct El.	0.2 Pct YS(MPa)	UTS(MPa)	Pct El.
2	121 (4)	204 (23)	6.9 (2.3)	140 (4)	230 (28)	8.7 (3.9)
6	106 (3)	173 (17)	5.2 (1.5)	116 (3)	195 (14)	5.8 (1.3)
10	87 (2)	123 (5)	2.8 (1.7)	96 (5)	131(8)	1.9 (0.6)

processes in pore-free regions, where other microstructure features are expected to play a greater role, were also investigated.

D. Fracture Process at the Microstructure Level

Microscopic examination of failed tensile test specimens revealed that cracks form predominately in the eutectic microconstituent adjacent to pores, as shown in Figure 11. This behavior was observed in all sections and was independent of the porosity size or distribution and distance from the fracture surface. The micrographs shown here are representative of sections from the 6-mm plates for both AM50 and AM60 and indicate that cracking occurred at multiple locations throughout the eutectic network. The linking of small, closely spaced cracks is also observed.

Observations of damage accumulation made *in situ* further confirmed this behavior, and crack initiation in the eutectic microconstituent was observed in both AM50 and AM60 specimens (Figure 12). The test specimen machined from the porosity-free region showed eutectic phase cracking during *in-situ* bend testing but did not fail in the test fixture at the maximum strain possible. Specimens from the high porosity volume fraction region failed at much lower surface strains and they, too, showed cracking in the eutectic region. In the latter case, large amounts of porosity were already present on the surface and most likely in the interior of these specimens.

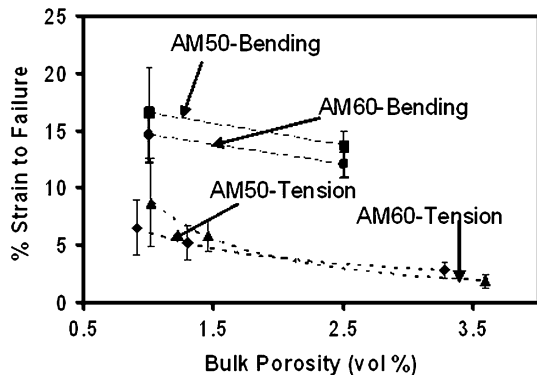


Fig. 8—Variation of tensile ductility and bend test strains to failure with bulk porosity for both AM50 and AM60.

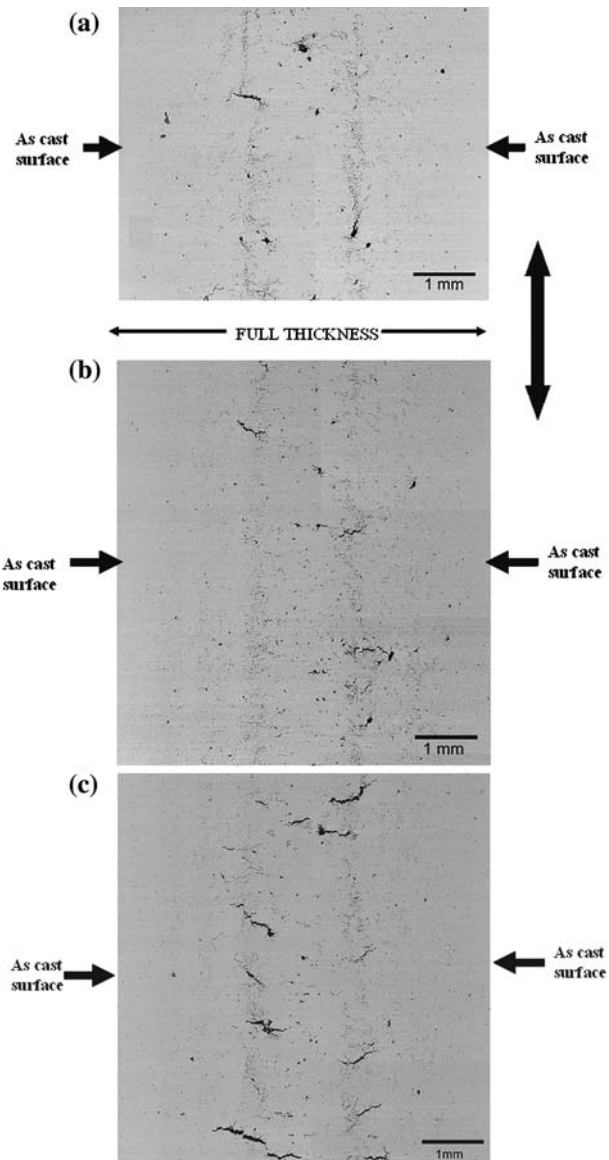


Fig. 9—Photomicrographs in backscattered electron mode showing damage accumulated in three different AM50 test specimens' full thickness with as-cast surface intact on sides after different strain levels of (a) 1 pct, (b) 3 pct, and (c) 4.5 pct. The direction of tensile testing is shown by the arrow on the top and was imaged in the backscattered electron mode.

IV. MODEL FOR DUCTILITY PREDICTION BASED ON ALLOY CHARACTERISTICS

Our phenomenological observations at the macrolevel clearly showed that cracks are initiated even at low

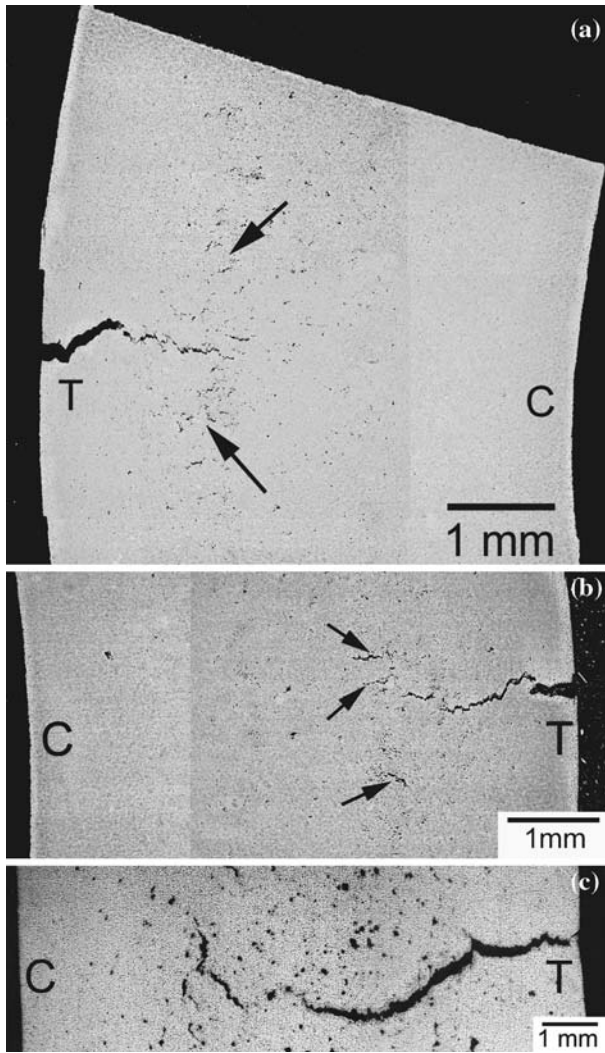


Fig. 10—Representative photomicrographs (full thickness) showing different active zones of failure in (a) and (b) 6-mm AM50 plate with failure occurring at the outer fiber and (c) a 10-mm AM60 plate showing cracks propagating from the plate interior to the outside fiber. (Note: C denotes the compressive side, and T indicates the tension side in the bend specimen.)

strains due to coalescence of microcracks initiated at micropores in the PSZs. Cracks form at multiple locations and eventually a few of these grow, coalesce, and lead to eventual failure. This sequence of failure can be characterized by a modified Brown–Embury model that analytically predicts fracture strain from information such as crack size, crack-tip radius, volume fraction of porosity, and elastic modulus of the alloy.^[29] The original Brown–Embury model^[28] correlates fracture strain only to the volume fraction of the porosity and assumes that pores are uniformly deformed in tension. It does not take into consideration any localized deformation that would depend on the local porosity characteristics.

The modified Brown–Embury model takes into account the local porosity characteristics such as local crack-tip radius and crack size in different regions of the specimen to determine the critical local strains that will

cause fracture in these regions of the specimen. The model assumes that cracks will propagate until the distance between the two cracks is equal to the critical plastic zone size. The critical strain at which this occurs is given by

$$\epsilon_f^p = \frac{2\sigma_y^p r}{E_P \rho} \left[\left(\frac{2\pi}{3f_P} \right)^{1/2} - \frac{\pi}{2} \right] \quad [1]$$

where ϵ_f^p is the fracture strain, σ_y^p is the yield strength, r is the mean pore radius, ρ is the crack tip radius, f_P is the volume fraction of pores, and E_P is the elastic modulus of the material with porosity.

The model predictions agree well with the tensile test data for both AM50 and AM60, as shown in Figure 13. Importantly, the trends predicted by the model (dotted line) follow closely the observed dependence of ductility on porosity volume fraction. The moduli of elasticity and yield stress were obtained from tensile tests (Table III). Cracks sizes, r , of 300 to 400 μm and crack tip radii, ρ , of 3 to 4 μm were assumed for the calculations and represent reasonable estimates for these alloys, based on the observations in this study. Here, the term crack size

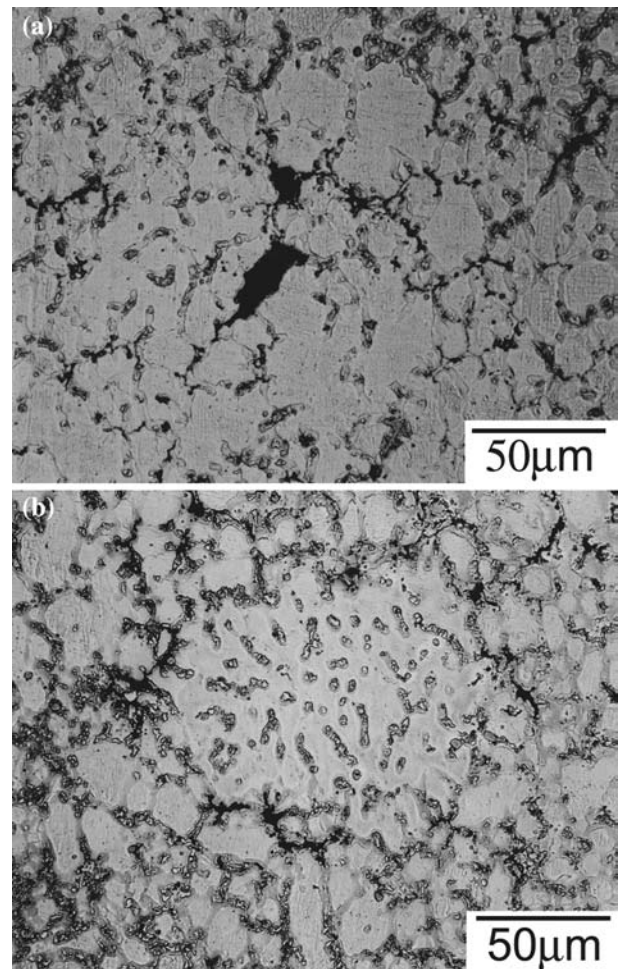


Fig. 11—Cracking of the eutectic region as observed in failed tensile test 6-mm plates: (a) AM50 and (b) AM60.

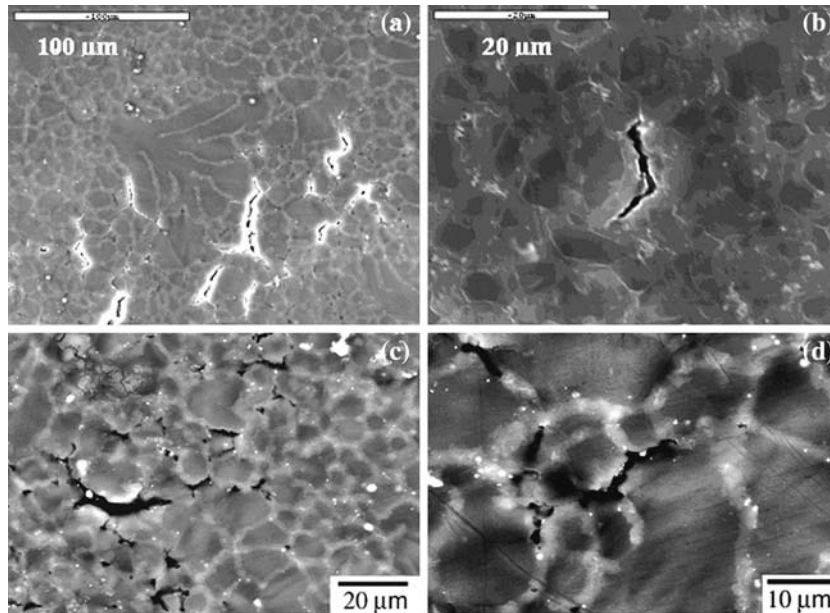


Fig. 12—Micrographs taken *in-situ* while bending for AM60 specimens from (a) higher pore volume fraction region, (b) pore free skin region showing eutectic cracking, and (c) and (d) more evidence of eutectic phase cracking in backscattered electron mode.

refers to long sharp elliptical cracks that form early in the deformation process. Although the value of r/ρ can be considered a fitting parameter in the model, the trend predicted by the model is similar to that observed experimentally and accurately predicts the nonlinear decrease in ductility with increasing bulk volumetric porosity for both AM50 and AM60.

The model can also be used to understand differences in the failure processes and resultant ductilities for different alloys and thicknesses of the die-cast plates. For example, if the r/ρ term is fixed, the variation of yield strength, σ_y^p , and the volume fraction of pores, f_P , determine the predicted strain at fracture. Between the 2- and 10-mm plates, σ_y^p increases by a factor of 2 (Table III) and the porosity term contribution to critical strain at failure decreases by a factor of 1.5. For the case of plate thickness, when other parameters are fixed, ductility is

dependent on the volume fraction of porosity as $\epsilon_f^p = F(f_P)$.

Conceptually, if we consider a cross section from the neutral axis of the plates toward the edge, we can profile the porosity variation along a line joining the neutral axis with the outer tensile fiber, as shown in Figure 14(a). This local porosity variation can then be used to predict the local fracture strain for both 6- and 10-mm-thick plates (Figure 14(b)) using the Brown–Embury model. In Figure 14(a), the symbols represent approximations of porosity (Figure 14(a)) and resulting calculations of fracture strain (Figure 14(b)). Comparison of the local fracture strain values predicted by the model to the local applied strain (at the fracture load) can be used to explain the observed behavior. For the 10-mm plates, the local applied strains in the plate interior are predicted to be much higher than the strains necessary for fracture, consistent with the observation that cracks form first in the interior and propagate to the specimen surface. However, for the 6-mm-thick plates, the local applied strains are generally comparable to the predicted local fracture strains in the plate interior. Hence, we would expect the first failure in the near-surface high strain region, as observed experimentally; although the local applied strains are also predicted to be greater than the local fracture strain in the PSZ for the 6 mm thick plate, which explains the multiple crack formation in this zone (Figure 10). However, because the PSZ is surrounded by high toughness, pore-free material, these cracks do not grow and do not cause failure.

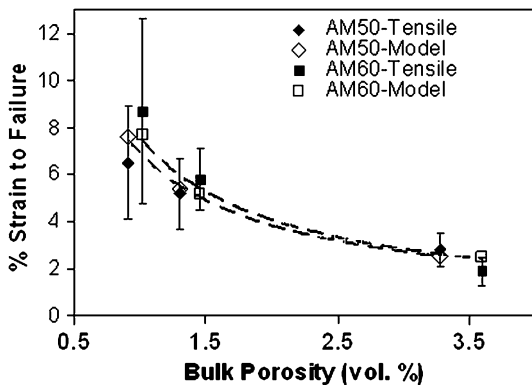


Fig. 13—Tensile ductility as a function of pore volume fraction. Comparing experimental data obtained from tensile testing with the analytical model (dotted line) for both AM50 and AM60.

V. DISCUSSION

Increasing section thickness results in a considerable decrease in tensile properties for the die-cast plates used

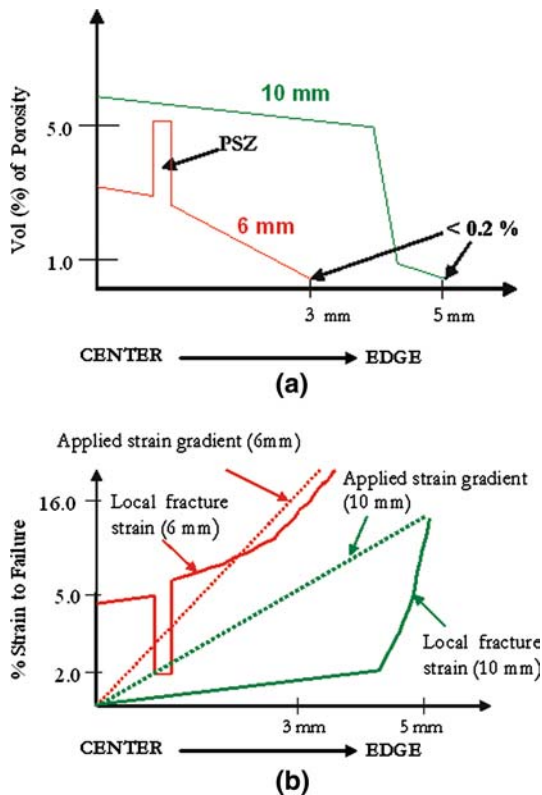


Fig. 14—Qualitative extension of the modified Brown-Embury model to the bend loading case: (a) map of porosity variation from the neutral axis to the outer fiber with some quantitative porosity estimates from image analysis, and (b) corresponding fracture values quantitatively predicted by the model compared to the applied strain gradient in bending at the nominal fracture loads of 6- and 10-mm-thick samples.

in the present study. The trends observed are in agreement with the observations of Stich and Haldenwanger^[21] and Schindelbacher and Rösch,^[22] who show that yield strength, ductility, and ultimate tensile strength decrease linearly with increasing section thickness. In contrast, the ductility and yield strength increase observed by Rodrigo *et al.*^[6] and Bowles^[8] with increasing section thickness does not agree with our results. These conflicting trends arise because microstructures, including porosity levels and distributions, are likely different in each of these studies because of the varying process parameters, specimen size, and shape for the alloys examined. The slightly higher tensile ductility observed in the present study for the 2- and 6-mm AM60 plates, compared to the AM50 plates, is probably the result of a more uniform distribution of porosity in the AM60 plates for these section thicknesses, as is evident by comparing Figures 6(a) and (b). Also, while it is important to note that the as-cast surface was removed from two specimen edges in machining tensile specimens, it is unlikely that this would significantly alter the observations on the role of section thickness on ductility. However, the absence of near-surface regions could possibly explain the slightly lower observed mechanical properties of the current study, compared to those reported in the literature for these alloys.^[2,5-8]

For 10-mm plates, we observed very low ductility of approximately 2.5 pct for both AM50 and AM50, which suggests that a bulk porosity greater than 3 vol pct would result in very low ductility in these alloys. This result agrees with previous studies,^[17,18] where for porosity in excess of 3 vol. pct, such low ductility values have been reported. If porosity levels can be maintained less than approximately 1.5 vol pct, it may be possible to control process parameters to eliminate the formation of PSZs. Presumably, this would result in a significant increase in ductility by reducing the localized nature of damage accumulation.

Our phenomenological findings indicate the following:

- microcracks initiate from micropores and coalesce, leading to formation of long sharp cracks in the PSZs even at low strain levels; and
- eutectic microconstituent cracking occurs at multiple locations in both tension and bending and is the mechanism by which crack propagation from pores occurs.

Porosity segregation zones have a deleterious effect on mechanical properties, as recently shown by Sannes and co-workers,^[11] and the progressive strain tests in the present study further demonstrate the impact these zones have on ductility, even at low strain levels. Sannes and co-workers^[11] report an approximate 45 pct decrease in ductility for the specimens possessing PSZs. This is approximately the level of decrease in ductility we observe in our plates, compared to literature for similar cross sections not containing PSZs.^[6] As mentioned previously, it is the early linkage of microcracks initiating from micropores that leads to the formation of the critical crack that eventually propagates to failure.

In bending, however, the highest nominal strains exist near the specimen surface and decrease linearly toward zero at the neutral axis of the bend specimens. For both 6- and 10-mm-thick plates, much higher ductility is observed in bending, especially for the 10-mm-thick plates, for which we observe a 400 pct increase in ductility. This suggests that the near-surface region is the determining microstructural feature controlling ductility in bending and that eutectic cracking in the near-surface region is critical in the onset and accumulation of damage during bending.

A competing pore-rich interior, though subjected to lower strain levels, can be detrimental, as observed for the 10-mm-thick plates, and can lead to a different failure sequence. Coalescence of microcracks to form a macrocrack in the plate interior of the 10-mm-thick plates, and subsequent propagation of the coalesced crack, or cracks, to the tensile surface, is the observed damage sequence leading to failure. For the 6-mm-thick plate, damage occurs in the PSZ, but, because the adjacent regions have much lower porosity, crack propagation outside the pore-rich zone is more difficult. Hence, as predicted by the model, the eventual failure that initiates in the near-surface region occurs by microcrack formation and linkage in the eutectic constituent. Previous investigations for AZ91 alloy showed evidence of brittle eutectic constituent cracking, but this

alloy has a more continuous eutectic network and higher volume fraction of the β -Mg₁₇Al₁₂ phase than the alloys studied here.^[8,24] In the present work, examination of longitudinal sections of AM50 and AM60 specimens that failed in tensile tests, combined with observations of damage accumulation in *in-situ* bend tests, reveals that large numbers of microcracks form in the eutectic regions both near to and remote from the final failure/fracture regions. These observations indicate the importance of eutectic constituent cracking in the fracture processes in these alloys and further confirm the critical role of the eutectic constituent in the failure process.

The modified Brown–Embury model presented here is more representative of the macroscale events in plates having PSZs and may be less appropriate for castings with no segregation zones or lower porosity levels. The absence of macroscale defects, such as porosity, implies a greater importance of microscale damage accumulation processes. Hence, eutectic microconstituent cracking is expected to play a more dominant role in the fracture processes, which will depend on the relative rates of damage accumulation in different regions of the microstructure during straining. Porosity segregation will play a dominating role in the fracture process and in determining ductility, but this will also depend on the mode of loading (*e.g.*, bending *vs* tension). If the PSZ is absent in the casting or this region has lower strains, as in bending, then eutectic microconstituent cracking becomes more important, if not the dominating factor. In such cases, the ratio of crack size and crack tip radii for the eutectic microcracks would be a more appropriate parameter to model ductility in die-cast magnesium alloys.

VI. CONCLUSIONS

1. Increases in section thickness lead to a considerable decrease in ultimate tensile strength, yield strength, and ductility in both tensile and bend loading conditions.
2. Heterogeneous distributions of porosity resulting in the formation of PSZs have the most deleterious effect on properties by serving as regions of relatively easy crack coalescence and propagation to fracture.
3. Crack formation in the eutectic microconstituent adjacent to pores is the primary mechanism of matrix damage in pore-containing regions. In pore-free regions, crack formation also occurs in the eutectic microconstituent. For both regions, volume fraction and morphology of the constituent phases can be expected to influence ductility.
4. A significant increase in the strain to fracture in bending was observed, compared to that observed in tensile tests. There is a corresponding change in the damage accumulation sequence between 6- and 10-mm-thick plates that is a direct result of the size and distribution of the heterogeneous porosity. For the

6-mm plates, failure initiated in the near-surface region, while failure initiated in the pore-rich interior for the 10-mm plates.

ACKNOWLEDGMENTS

The authors acknowledge funding from the Ford Motor Company and the following people at the Ford Materials Research Laboratory. We are thankful to Drs. James M. Boileau and Steve Harris for help with the *in-situ* bend tests. Helpful discussions with Dr. Joy Hines and Larry A. Godlewski are also gratefully acknowledged.

REFERENCES

1. D. Magers and J. Willekens: *Werkstoff-Informationsgesellschaft*, in *Magnesium Alloys and Their Applications*, B.L. Mordike and K.U. Kainer, eds., Wolfsburg, Germany, 1998, pp. 247–52.
2. D.J. Sakkinen: SAE Technical Paper No. 940779, SAE, Detroit, MI, 1994.
3. B.L. Mordike and T. Ebert: *Mater. Sci. Eng.*, 2001, vol. A302, pp. 37–45.
4. D.F. Allsop and D. Kennedy: *Pressure Die Casting Part 2: The Technology of the Casting and the Die*, Pergamon Press, New York, NY, 1983.
5. H. Mao, J. Brevick, C. Mobley, V. Chandrasekar, D. Rodrigo, M. Murray, and R. Esdaile: SAE Technical Paper No. 1999-01-0928, SAE, Detroit, MI, 1999.
6. D. Rodrigo, M. Murray, H. Mao, J. Brevick, C. Mobley, V. Chandrasekar, and R. Esdaile: SAE Technical Paper No. 1999-01-0927, SAE, Detroit, MI, 1999.
7. T.K. Aune, D.L. Albright, and H. Westengen: SAE Technical Paper No. 900792, SAE, Detroit, MI, 1990.
8. A.L. Bowles: Ph.D. Thesis, The University of Queensland, Queensland, Australia, 2002.
9. R.M. Wang, A. Eliezer, and E.M. Gutman: *Mater. Sci. Eng. A*, 2003, vol. 355(1–2), pp. 201–20.
10. Z. Shan and Arun M. Gokhale: *Mater. Sci. Eng. A*, 2003, vol. 361, pp. 267–74.
11. S. Sannes, H. Gjestland, H. Westengen, H.I. Laukli, and O. Lohne: SAE Technical Paper No. 2003-01-0183, SAE, Detroit, MI, 2003.
12. A.K. Dahle, Y.C. Lee, M.D. Nave, P.L. Schaffer, and D.H. St. John: *J. Light Met.*, 2001, vol. 1, pp. 61–72.
13. A.K. Dahle, S. Sannes, D.H. St. John, and H. Westengen: *J. Light Met.*, 2001, vol. 1, pp. 99–103.
14. A.K. Dahle and D.H. St. John: *Acta Mater.*, 1999, vol. 47, pp. 31–41.
15. Haiping Cao and Magnus Wessén: *11th Magnesium Automotive and End User Seminar*, Aalen, Germany, 2003.
16. C.D. Lee: *Met. Mater. Int.*, 2002, vol. 8(3), pp. 283–88.
17. Z. Liu, L. Chen, H. Zhao, Y. Wang, Z. Wang, and F. Klein: *Metall.*, 2000, vol. 54, pp. 122–25.
18. A.L. Bowles, J.R. Griffiths, and C.J. Davidson: *Magnesium Technology 2001*, New Orleans, LA, 2001, J. Hryn, ed., TMS, Warrendale, PA, 2001, pp. 161–68.
19. M. Easton, T. Abbott, and C. Caceres: *Mater. Sci. Forum*, 2003, vols. 419–422, pp. 47–52.
20. T. Abbott, M. Easton, and W. Song: *Mater. Sci. Forum*, 2003, vols. 419–422, pp. 141–46.
21. A. Stich and H.G. Haldenwager: *Magnesium 2000*, Proc. 2nd Israeli Int. Conf. on Magnesium Science and Technology, Dead Sea, Israel, 2000, E. Aghion and D. Eliezer, eds., 2000, pp. 27–34.
22. G. Schindelbacher and R. Rosch: *Werkstoff-Informationsgesellschaft*, in *Magnesium Alloys and Their Applications*, B.L. Mordike and K.U. Kainer, eds., Wolfsburg, Germany, 1998, pp. 247–52.

23. B.J. Coultres, J.T. Wood, G. Wang, and R. Berkmortel: *Magnesium Technology 2003*, H.I. Kaplan, ed., San Diego, CA, 2003, TMS, Warrendale, PA, 2003, pp. 45–50.
24. Y.Z. Liu, Q.D. Wang, W.J. Ding, X.Q. Zeng, and Y.P. Zhu: *Mater. Lett.*, 2000, vol. 44, pp. 265–68.
25. D. Regener, E. Schick, I. Wagner, and H. Heyse: *Materialwissenschaft Werkstofftechnik*, 1999, vol. 30, pp. 525–32 (in German).
26. Haiping Cao and Magnus Wessén: private communication.
27. M.D. Nave, A.K. Dahle, and D.H. St John: *Magnesium Technology 2000*, Nashville, TN, 2000, H.I. Kaplan, J. Hryn, and B. Clow, eds., TMS, Warrendale, PA, 2000, pp. 233–42.
28. L.M. Brown and J.D. Embury: *Proc. Int. Conf. on Microstructure and Design of Alloys*, London, 1973, Institute of Metals and Iron and Steel Institute, London, 1973, vol. 1, pp. 164–69.
29. J.Y. Jung: *Phil. Mag. A*, 2002, vol. 82(11), pp. 2263–68.